Int. J. Heat Mass Transfer. Vol. 33, No. 10, pp. 2311–2328, 1990
Printed in Great Britain

0017-9310/90 $3.00 + 0.00


# The effects of sharp corners on buoyancy-driven flows with particular emphasis on outer boundaries

KAMBIZ VAFAI and JAVAD ETTEFAGH
Department of Mechanical Engineering, The Ohio State University, Columbus, OH 43210, U.S.A.

(*Received* 15 *September* 1989 *and in final form* 4 *January* 1990)

**Abstract**—The effects of sharp corners and the far field boundary conditions on vorticity generation and flow instabilities are discussed. The importance of the far field boundary conditions and the interaction between the controlling variables are discussed and an in-depth analysis of the fluid flow and vortex interaction in the open-ended cavity is presented. The formation of a thermally stratified region and its role in influencing the thermal instabilities is discussed. The transient behavior of the flow field through the formation of vortices and the opposing interactions of the buoyant and suction mechanisms leading to an oscillating central vortex and overshooting and oscillations in the heat transfer process are analyzed. Finally, the effects of the geometric and thermophysical parameters as well as the influence of the Rayleigh number and different temperature levels are thoroughly explored.

## 1. INTRODUCTION

IN THE buoyancy-driven convection, the problems can be categorized in two different ways depending on whether the density gradient is parallel or normal to the gravitational field. If the density gradient is normal to the gravitational field, convective motion starts almost immediately following the initial conduction. But, if the density gradient is parallel and opposed to the gravitational field, convection will occur only if the density gradient is large enough. The significance of fluid motions, resulting from buoyancy forces, in many engineering applications has prompted many researchers to carry out numerous studies to improve their understanding of the governing processes. Among these investigations, two-dimensional natural convection in enclosures or cavities has been the subject of many studies due to its important role in many modern technologies. These studies have been applied to several, different problems such as heat transfer across unventilated air gaps, multi-layered walls, design of efficient fire detection systems, analysis of the solar collectors, and many environmental and geothermal flow processes.

While two-dimensional natural convection in enclosures constitutes a very large portion of these investigations, a related but more complex problem on partial enclosures and open cavities, has received very little attention. One of the reasons for this asymmetry can be traced to the difficulty in specifying the proper boundary conditions for an open cavity configuration resulting from its significantly more complex geometry. Since it seems almost impossible to impose known physical conditions in the aperture plane, all the numerical studies included calculations in an enlarged computational domain and therefore, partly overcame the problem of unknown physical conditions at the opening. The present study shows that the extent of the enlarged computational domain has a more pronounced effect on the results than previously anticipated by other researchers. The results of this study clearly show the importance of buoyant forces on the heat transfer process in an open cavity. Furthermore, by a rigorous examination of the transient development of the flow field the present investigation will constitute one of the very few works that have illustrated the transient flow and thermal characteristics of an open cavity configuration. Among the previous studies Penot [1] demonstrated the dependence of thermal losses on cavity orientation including the existence of large scale variations in the flow for specific conditions of Grashof number and inclination angle. LeQuere *et al.* [2] studied the same configuration with variable properties using primitive variables. They found that flow unsteadiness arises for values of $Gr > 10^6$ and that the thermal losses diminish with increasing values of the inclination angle resulting from stable stratification of the flow and the subsequent decrease in the unsteadiness. They also found that the flow field approaching the open cavity depends on the far field boundary specifications. LeQuere *et al.* [2] had mentioned that the flow field within the open cavity and in the aperture plane is determined mainly by the local heat transfer effects and is relatively insensitive to the far field specifications if the far field boundary is at a distance of two cavity heights or more from the aperture plane. However, based on our analysis, these types of extensions were quite inadequate for the present investigation.

Unlike the previous studies that involved a heated bottom wall, Chan and Tien [3] examined natural convection in a two-dimensional open cavity with insulated top and bottom walls. In their study, steady flow characteristics were explored up to a Grashof number of $10^9$. They reported that the near field solu-

## NOMENCLATURE

$d$ length of the cavity [m]
$H$ open cavity height [m]
$Nu_c$ Nusselt number for the cavity
$Pr$ Prandtl number, $\nu/\alpha$
$Ra$ Rayleigh number, $g\beta H^3\Delta T/\alpha\nu$
$T$ temperature [K]
$u$ non-dimensionalized $x$-component velocity
$v$ non-dimensionalized $y$-component velocity
$x$ non-dimensionalized horizontal coordinate
$y$ non-dimensionalized vertical coordinate.

Greek symbols
$\alpha$ thermal diffusivity [$m^2 s^{-1}$]
$\beta$ thermal expansion coefficient of fluid [$K^{-1}$]
$\zeta$ vorticity
$\theta$ dimensionless temperature
$\mu$ dynamic viscosity [$kg m^{-1} s^{-1}$]
$\nu$ kinematic viscosity [$m^2 s^{-1}$]
$\rho$ fluid density [$kg m^{-3}$]
$\psi$ stream function.

Subscripts
1 lower block
2 upper block
$\infty$ free stream.

tions inside the open cavity and close to the opening are satisfactory if reasonable boundary conditions are set far away from the opening. They also concluded that this approach is necessary since the boundary conditions at the opening are not specific and the flow patterns in the region just outside the opening are also of interest.

While the study of natural convection in an open cavity configuration has received very little attention, the analysis of thermally-driven flows in open-ended cavities has not yet been studied. The only investigation in this area has been by Ettefagh and Vafai [4] who performed a numerical investigation of natural convection in open-ended cavities with a porous medium. However, the natural convection in regular open-ended cavities has not been studied. Although by utilization of the symmetry consideration, the geometry of half of an open-ended configuration will have a superficial similarity to the open cavity, the temperature boundary conditions on the open-ended cavity and the physics of the process are very different. Since the flow and temperature fields within the open cavity are determined mainly by local heat transfer events, the significance of the different temperature boundary conditions also become more apparent. In this work the transient Nusselt number which represents the heat transfer process is shown to exhibit an overshooting followed by damped oscillations around its steady state value. Furthermore, by presenting a thorough and in-depth analysis of the specifications of the far field conditions, etc. on the heat transfer and fluid flow inside the open-ended cavity; the present investigation will also directly extend and clarify several unsolved issues in the open cavities.

## 2. ANALYSIS

Consider the two-dimensional open-ended cavity of length $d$ and height $H$ shown in Fig. 1. The lower block and upper block temperatures of the slot are maintained at $T_1$ and $T_2$, respectively, while the surrounding fluid communicating with the open-ended cavity is at an ambient temperature $T_\infty$ which is lower than $T_1$ and $T_2$. The vertical portions of both blocks are assumed to be adiabatic. The equations governing the conservation of mass, momentum and energy formulated in terms of vorticity, stream function, and temperature with the fluid medium regarded as Boussinesq-incompressible are written as

$$\frac{\partial\xi}{\partial t}+u\frac{\partial\xi}{\partial x}+v\frac{\partial\xi}{\partial y}=Pr\cdot\nabla^2\xi-Pr\cdot Ra\cdot\frac{\partial\theta}{\partial x}$$

$$\nabla^2\psi=\xi$$

$$\frac{\partial\theta}{\partial t}+u\frac{\partial\theta}{\partial x}+v\frac{\partial\theta}{\partial y}=\nabla^2\theta$$

where

$$u=\frac{\partial\psi}{\partial y},\quad v=-\frac{\partial\psi}{\partial x},\quad \xi=\frac{\partial u}{\partial y}-\frac{\partial v}{\partial x}.$$

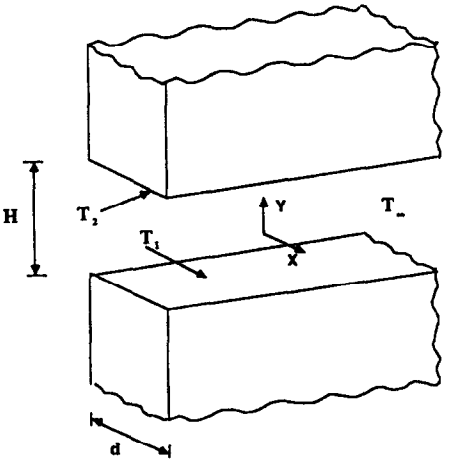


FIG. 1. Schematic of an open-ended cavity.

The equations were made dimensionless by scaling the length variables by the open cavity height, $H$, the time by $H^2/\alpha$, where $\alpha$ is the thermal diffusivity of the medium, temperature by the temperature difference between lower block and the ambient and the velocity by $\alpha/H$. The resultant three non-dimensional parameters in the above equations are the Rayleigh number defined as $Ra = g\beta H^3\Delta T/\alpha\nu$, the Prandtl number, $Pr = \nu/\alpha$ and the aspect ratio, $A = H/d$. In the above expressions $g$ is the gravitational acceleration, $\beta$ the coefficient of volume expansion, and $\nu$ the kinematic viscosity of the fluid medium. As mentioned before, the treatment of the far field boundary conditions in the open cavity geometry requires careful consideration. The open boundary conditions were approximated by specifying zero normal gradients for the velocities and temperature at these locations. The above approximations supplied enough accuracy (as will be discussed in more detail) provided that the computational domain is extended far enough. In this investigation, many numerical runs were carried out in which several, different far field boundary conditions plus different extensions of the open boundaries were examined. The numerical tests showed that the far field flow characteristics were quite sensitive to the type of boundary conditions which were used. The results also showed that, the flow and heat transfer characteristics inside the open-ended cavity and in its immediate surroundings did not alter significantly if the computational domain was extended at least 60 times the cavity height for cases with high Rayleigh number. It should be noted that these type of extensions are far more than what was previously considered being needed by other investigators. For example, LeQuere *et al.* [2], in relation to predicting laminar natural convection in a heated cavity (while they have noted that a realistic calculation of the far field flow pattern does call for careful attention to the specification of the far field boundary conditions) have used a maximum extension of only about twice the cavity height in specifying the outer boundary conditions.

To reduce the size of the computational domain, the expected symmetry condition was used at the centerline of the open-ended cavity. The validity of using the symmetry conditions at the centerline of the cavity was checked through a series of numerical runs. Specifically this was done by comparing the numerical results which were obtained for half of the open-ended cavity, using the symmetry conditions, vs the full numerical simulation of the entire open-ended cavity. As a result of the above-mentioned comparisons it became apparent that the use of the symmetry conditions on half of the open-ended cavity is equivalent to simulating the entire open-ended cavity. Furthermore, we also perturbed the flow and again observed a return to a symmetrical state. This was done by performing a number of separate runs using a series of different and asymmetrical initial conditions. The results of the runs were also used to show that the initial conditions do not have any influence on the steady state results.

The lower and upper block Nusselt numbers are defined as the ratio of actual heat transfer rate to pure conduction heat transfer rate. The rate of heat transfer across the open-ended cavity was calculated in terms of a cavity Nusselt number which represents the non-dimensional total rate of heat transfer from the entire cavity, and is given as

$$Nu_c = -A\int_0^{1/2}\left.\frac{\partial\theta}{\partial y}\right|_{y=-A/2}\mathrm{d}x + \frac{A}{\theta_2}\int_0^{1/2}\left.\frac{\partial\theta}{\partial y}\right|_{y=A/2}\mathrm{d}x.$$

The presence of a large computational domain and the complex interactions between the boundary layers along the blocks and the rest of the flow field, and the presence of an oscillating vortex inside the cavity at higher Rayleigh numbers (discussed in detail later) demanded the use of an efficient and accurate algorithm for the present problem. This was established by developing:

(a) a very stable implicit finite differencing scheme in which at each time step the internal and the boundary nodes for $\psi$ or $\theta$ were updated within one sweep of the computational domain;
(b) a highly vectorized algorithm;
(c) a variable grid structure.

Figure 2 displays the non-uniform grid distribution for the portion of the domain which concentrates on the cavity and its immediate surroundings. The non-uniform grid network used in this work possesses a *very fine* grid structure near the symmetry line which gradually converts to a *fine* grid structure inside the cavity. In the extended computational domain, the grid distribution is fine near the vertical portions of the cavity and then it gradually becomes coarser towards the far field. In this work the grid distribution

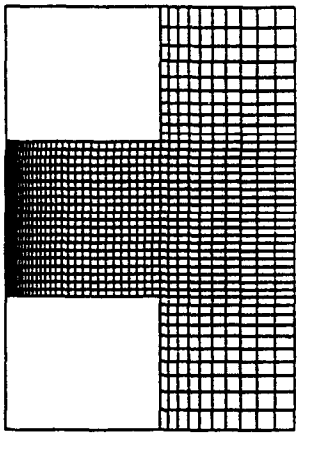

FIG. 2. The non-uniform grid distribution for the portion of the computational domain which concentrates on the cavity and its immediate surroundings.

was chosen such that the second-order accuracy would be preserved. This required that the variable grid space would undergo a gradual increase or decrease such that the truncation error for the utilized grid system would be locally of the same order of magnitude as that which would occur in a uniformly spaced grid system. It should be noted that the mesh layout covers a far larger region than what is shown in Fig. 2. However, for clarity, only the cavity and its immediate surroundings are shown since the inclusion of the entire region in Fig. 2 would obscure the mesh layout pattern in the cavity region.

The two parabolic equations (vorticity and energy equations) are solved in a variable grid mesh by a modified *ADI method* which incorporates the upwind differencing and accounts for the convective instabilities. The diffusion terms were approximated in the non-uniform grid system ($x_{i+1}-x_i=\Delta x_i$, $y_{j+1}-y_j=\Delta y_j$) by a central differencing scheme. The initial conditions used in this work were: a uniform temperature fluid (at the ambient temperature) which is initially at rest. Aside from being quite basic, these type of initial conditions, were motivated by physical considerations as they prevail in a variety of practical problems. Since the transient simulation of the flow and heat transfer characteristics were among the major concerns in this work, the same initial conditions, i.e. fluid being at rest and having the same temperature as the surroundings were used for all the numerical results which were presented in this work. By performing a series of separate runs, using different initial conditions it was ascertained that the initial conditions do not have any influence on the steady state results. At each time step, the elliptic equation (*Poisson equation*) is solved by an *extrapolated Jacobi scheme*, an iterative method with optimum over-relaxation.

The vorticity is then advanced in time using methods analogous to those used on the energy transport equation. The stream function is then updated by the *extrapolated Jacobi scheme*. The heat flux is calculated by three point differencing of the temperature gradients at the walls, and the cavity Nusselt number is found by numerical integration using *Simpson's rule*. It is assumed that the steady state conditions have been reached when the following convergence criteria:

$$\frac{\phi_{i,j}^{n+1}-\phi_{i,j}^{n}}{\phi_{i,j}^{n+1}} \leqslant 10^{-3}$$

for temperature, stream function, and vorticity have been met. In the above expression, $n$ refers to any particular time level and $\phi$ represents either one of the three dependent variables. In practice, the temperature and the stream function satisfy a more stringent convergence criteria than what is given in the above expression.

The vorticity at sharp corners require special consideration. Several methods of handling this corner vorticity are discussed in Roache [5]. Such discontinuous treatment for the vorticity evaluation were suggested by Thom and Apelt [6], Roache and Mueller [7], and Kacker and Whitelaw [8] and used by several different researchers. Here to model as appropriately as possible the mathematical limit of a sharp corner, the method of discontinuous vorticity values is used. The bifurcation of the vorticity at the corners is essentially handled through introduction of two different vorticity values. These are $\omega_a$ and $\omega_b$, where both are evaluated by using the no-slip wall equation, but $\omega_a$ is evaluated by considering the corner being part of the horizontal wall while $\omega_b$ is evaluated by considering it to be part of the vertical section of the block. Then in an interior point difference equation, $\omega_a$ or $\omega_b$ is used for the corner vorticity depending on the differencing direction. The temperature condition at the sharp corners also requires special attention. Since there are two kinds of temperature boundary conditions (specified temperature on horizontal portion and adiabatic on vertical portion) imposed on the corner, a multi-valued procedure similar to vorticity evaluation is also used for the temperature differencing at the corners.

The proper magnitude of the time increment (used in the numerical calculations) was primarily dependent on the Rayleigh and the Prandtl numbers; once the proper extension of the computational domain was established. For example, a typical non-dimensional time increment used for the range of low to moderately high Rayleigh numbers, $Ra < 10^5$ (with air as the working fluid), was $10^{-3}$. However, for larger Rayleigh numbers, $Ra > 10^5$, the non-dimensional time increment had to be reduced to about $10^{-4}$ or lower. For fluids with higher Prandtl number, time steps of $10^{-4}$–$10^{-5}$ were used. To examine the dependency of the results on the chosen time interval, many numerical runs with smaller time steps were performed. All these runs resulted in identical solutions. During our investigations many different boundary conditions, such as constant values, first and second gradients of the stream function and the temperature field, were investigated in applying the outer boundary conditions. As a result of these extensive investigations, it was determined that the most representative set of boundary conditions are those which are depicted in Fig. 3.

## 3. RESULTS AND DISCUSSIONS

The influence of governing physical parameters such as the Rayleigh number, Prandtl number, and different temperature ratios between two blocks on the temperature and velocity distributions for the buoyancy-driven flows in open-ended cavities were thoroughly explored. The effects of geometric parameters such as aspect ratio of the open-ended cavity and the importance and influence of the far field con-

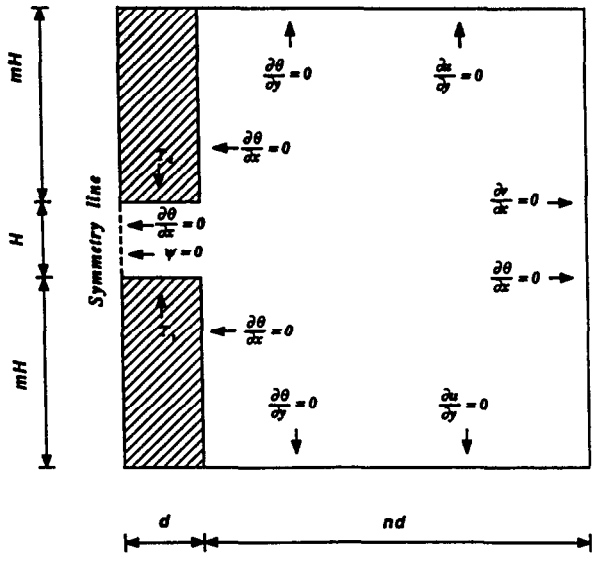


FIG. 3. Schematic of the problem with boundary conditions.

ditions on the flow and heat transfer characteristics within the open-ended cavity and its immediate surroundings were also examined. The bulk of the results were obtained for cases with the lower block surface temperature of $\theta_1 = 1$, the upper block surface temperature of $\theta_2 = 1$, an aspect ratio of $A = 0.5$, and using air as the working fluid. In all cases, the full transient behavior of the heat transfer characteristics inside the cavity were studied. To accurately detect the detailed information about the flow field especially for higher Rayleigh numbers, the variable mesh network having a mesh size of 0.01 (translating into 651 points) was used inside the open cavity for an aspect ratio of 0.5. The typical time increment used was $10^{-3}$ for air, and $10^{-4}$–$10^{-5}$ for fluids with higher Prandtl number.

The open boundaries were systematically extended in both directions and it was found that it was necessary to extend the computational domain at least 16 times the height of the cavity to eliminate the effects of the far field solution on the flow field and the heat transfer characteristics inside the open cavity and in its immediate opening. This extension was doubled for cases with $Ra > 10^4$ and tripled for cases with $Ra > 10^5$. It should be mentioned that the magnitude of this extension is in sharp contrast to the limited number of studies which were carried out on the partially closed cavity problem, i.e. Penot [1], LeQuere *et al.* [2], and Chan and Tien [3]. In these studies, the maximum extensions reported were only twice the height of the cavity. Based on our investigation, this was found to be quite inadequate. To illustrate the results of the flow and temperature fields inside the open cavity, only the portion which concentrates on the open-ended region and its close vicinity is presented. However, always, the much larger domain was used for numerical calculations and interpretation of the results. It should be noted that the values of isotherms start with 0.1 and are incremented by 0.1 for all figures throughout this work. The streamline contour values are set to zero on all solid boundaries and are incremented by two for all the steady results except Fig. 4, in which they are incremented by one.

### 3.1. *The effects of Rayleigh number*

As shown in Fig. 4(a) for $Ra = 10^3$, the heat transfer inside the open cavity is mainly by conduction. However, the convective heat transfer is surely not negligible as seen by the distortion of the isotherms at the opening. The hot buoyant fluid rises like a buoyant plume into the outside domain as it escapes from the restrictive horizontal top surface. Because of this 'ejection mechanism', caused by the energy transfer from the internal surfaces of the cavity to the fluid, the cold fluid from the outside creeps into the lower part of the open cavity and replaces the departing hot fluid. Even at this Rayleigh number the flow field inside the open cavity is not symmetric about the mid-height plane. This is because the 'ejection mechanism' acting on the hot exiting fluid gives rise to higher velocities associated with the departing flow than that of the entering flow. Hence, as a direct consequence of the conservation of mass, the cold incoming fluid occupies a larger part of the aperture plane than the hot exiting flow.

As the Rayleigh number increases from $10^3$ to $10^4$, the cold fluid penetrates further inside the open cavity. However, since the flow penetrates in the cavity from both sides with equal vigor, it is forced to turn around

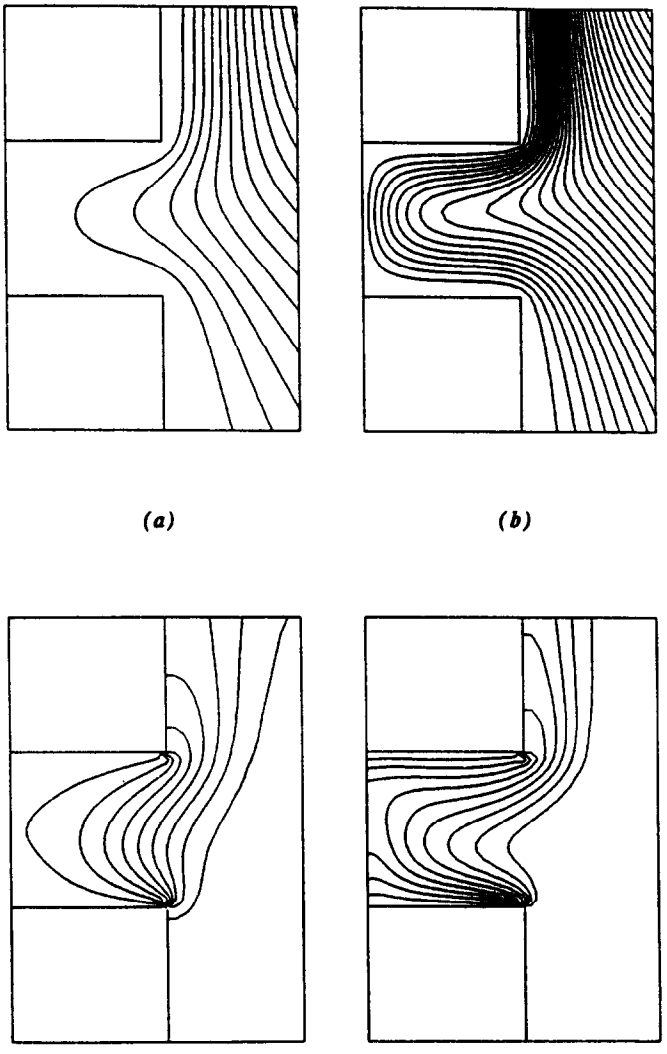


FIG. 4. Streamlines and isotherms for $\theta_2 = 1$, $A = 0.5$, $Pr = 0.71$: (a) $Ra = 10^3$, (b) $Ra = 10^4$ at steady state.

the centerline of the cavity. As shown in Fig. 4(b), the departing streamlines are spaced closer together along the vertical wall showing the higher speeds associated with the outgoing fluid. It also shows the early stages of the wall plume formation along the upper insulated wall. It should be noted that the interaction of the wall with the plume is to attract it as a result of the boundary layer formation on the wall. The approaching flow from the far field is sucked into the open cavity to fill the space left behind by the departing plume. At higher Rayleigh numbers, the cold creeping flow is sucked inside the open cavity at higher speed. This 'suction mechanism' is responsible for an almost parallel flow along the lower block. While this flow travels inside the open cavity, the fluid is heated along the lower block. Therefore, the fluid particles traveling along the lower block are subjected to two different driving mechanisms with respect to time. While the 'suction mechanism' gives rise to an almost parallel flow, the 'buoyant mechanism' forces the fluid elements to rise up in a direction which is opposite to that of the gravitational field. These different driving forces on the entering fluid are the cause of the 'oscillations' in the transient variations of the lower block Nusselt number which will be discussed in more detail later. Comparison of Figs. 4(a) and (b) shows that, as $Ra$ increases, the streamlines and isotherms become closely spaced together along both blocks. As a result of this higher temperature gradient, the heat transfer from the lower block increases. The heat transfer from the upper block which is mainly governed by conduction also increases. The comparison also shows that as $Ra$ increases, the horizontal temperature gradient in the upper part of the open cavity decreases, resulting in a thermally-stratified flow along the upper block.

As Rayleigh number increases further ($10^5$–$5 \times 10^5$), the cold incoming fluid enters the open cavity at much higher speeds and penetrates much further inside. As shown in Fig. 5(a), near the lower block, the streamlines and isotherms are more closely spaced together resulting in the formation of a thermal boundary layer along the block. The thickness of this thermal layer decreases with an increase in *Ra*, as seen in Fig. 5(b). Comparison of Fig. 5(b) with Fig. 5(a) and especially Fig. 4(b) shows that the thermally-stratified region in the upper part of the open cavity becomes more apparent with an increase in *Ra*. The comparison also shows that, as *Ra* increases, the outgoing fluid rises up at much faster speeds resulting in a thinner wall plume. Due to this thinner thermal boundary layer which is responsible for most of the heat transfer to the quiescent and far field fluid, the overall plume temperature decreases as *Ra* increases. The formation of a circulating flow region inside the open cavity as a result of viscous effects associated with high speeds of both incoming and outgoing flows is depicted in Fig. 6(b).

### 3.2. *Transient results*

Figures 7–9 show the transient behavior of the flow and temperature fields for the general case of the lower block temperature of $\theta_1 = 1$, the upper block temperature of $\theta_2 = 1$, an aspect ratio of $A = 0.5$, Prandtl number of $Pr = 0.71$, and the Rayleigh number of $Ra = 10^5$. For both primary and recirculating flows, the streamline contour values are set to zero on all the solid boundaries. These contour lines are incremented by two for all the transient results except in Fig. 7 in which they are incremented by one. Figure 7 clearly illustrates the effects of the sharp corners in vorticity generation. As a result of the flow over the external corners, two vortices rotating about the same axis are generated. As time progresses, the lower vortex moves up along the aperture plane while, the top vortex moves out of the upper corner of the opening as seen in Fig. 7. These vortices eventually combine and continue to move upward and away from the opening as shown in Fig. 8(a). In the early stages of the flow development ($0 \leqslant \tau \leqslant 9\Delta\tau$), the dominant heat transfer mechanism inside the open cavity is by

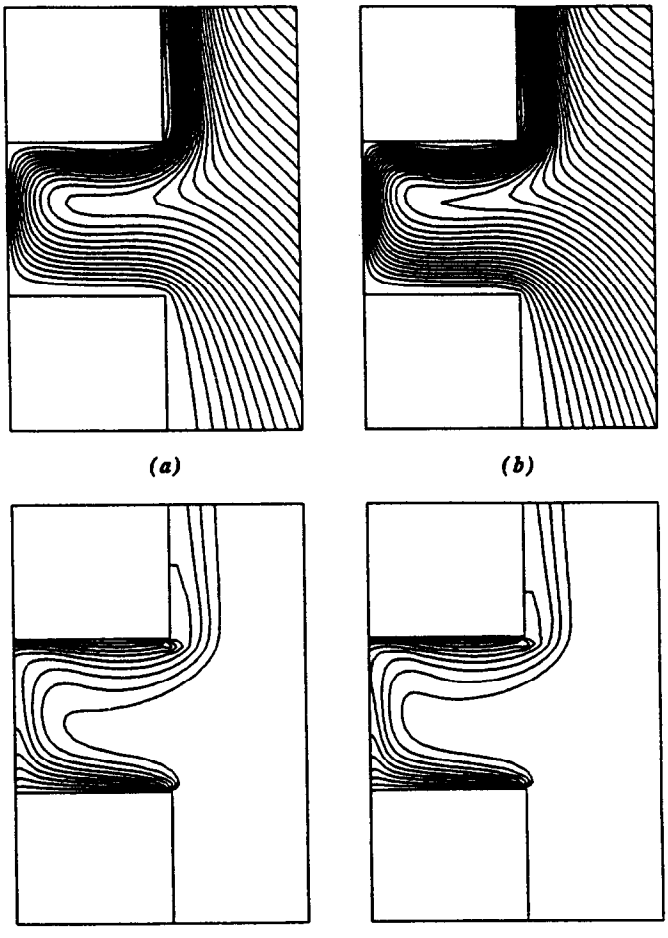


FIG. 5. Streamlines and isotherms for $\theta_2 = 1$, $A = 0.5$, $Pr = 0.71$ : (a) $Ra = 10^5$, (b) $Ra = 2 \times 10^5$ at steady state.

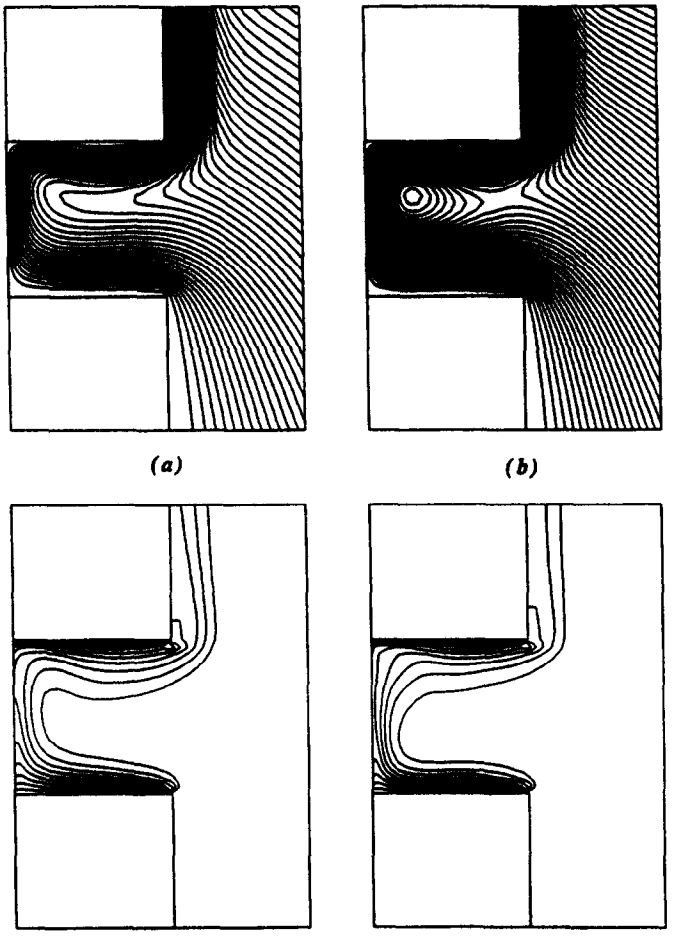


FIG. 6. Streamlines and isotherms for $\theta_2 = 1$, $A = 0.5$, $Pr = 0.71$: (a) $Ra = 3 \times 10^5$, (b) $Ra = 5 \times 10^5$ at steady state.

conduction, however, the contribution of the convective heat transfer near the opening is still present. Figure 7(b) illustrates the beginning of the formation of a weak secondary circulation along the lower block. The onset of this recirculating flow is the result of the viscous interaction between the primary flow and the stagnant flow which occupies the end portion of the cavity. Figures 7(c) and (d) show that, as the cold incoming fluid continues to penetrate further inside the open cavity, it is being opposed by the secondary flow which becomes stronger in time. This recirculating flow is responsible for the temperature inversion of the fluid inside the open cavity away from the opening as shown by the isotherms in Fig. 7(d). The secondary circulation continues to become stronger in time until it occupies the central half portion of the open-ended cavity as presented in Fig. 8(a). It should be noted that for the full cavity we have two vortices over the central portion of the open-ended cavity. The isotherms in Fig. 8(a) show that, the temperature of the fluid near the symmetry line is increased by the heat removal process of the secondary flow from the lower block. Simultaneously, due to the heat input from the secondary flow as it approaches the lower block, the temperature of the fluid in the central part of the open cavity increases even further. This is clearly seen by the shapes of the isotherms in Fig. 8(a). Hence, the horizontal temperature distribution of the fluid in the lower part of the open cavity exhibits a parabolic shape over the entire lower block. The heating process of the fluid by the secondary circulation continues to a point in time when the peak in strength of the recirculating flow is reached. After this time, due to an increase in the overall temperature of the fluid inside the open cavity, the strength of the recirculating flow begins to decay in time as shown in Figs. 8(b) and (c). This decline continues in time to a point after which it completely submits to the primary flow as it starts to occupy the entire cavity as illustrated in Fig. 8(d). Figure 9 presents different stages of the flow development in the period from the total decay of the secondary flow up to and including the steady state.

### 3.3. *The effects of Prandtl number*

To study the effects of the Prandtl number on the flow and temperature fields, two different working

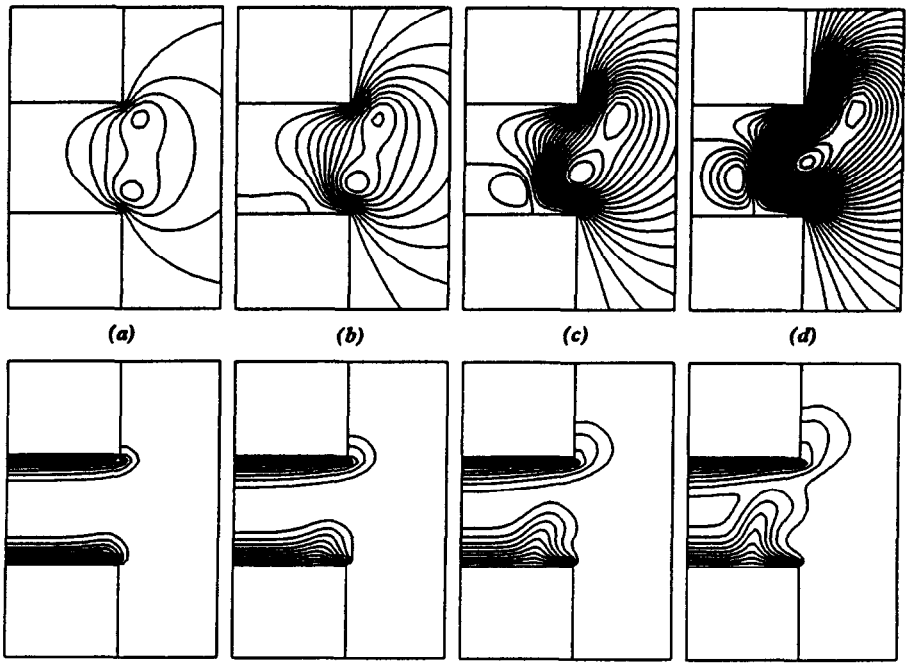


FIG. 7. Streamlines and isotherms for $\theta_2 = 1$, $A = 0.5$, $Pr = 0.71$, $Ra = 10^5$ at: (a) $\tau = 6\Delta\tau$, (b) $\tau = 9\Delta\tau$, (c) $\tau = 12\Delta\tau$, (d) $\tau = 15\Delta\tau$.

fluids other than air, namely water and heavy oil were used. The numerical results are presented for the general case of the lower block temperature of $\theta_1 = 1$, upper block temperature of $\theta_2 = 1$, aspect ratio of $A = 0.5$, and a Rayleigh number of $Ra = 10^5$. Figures 10(a)–(c) present the streamlines and isotherms for three different fluids with $Pr = 0.71$, 7.0, and 100 respectively. Comparison of the streamlines in Figs. 10(a) and (b) indicates that the flow field for the water ($Pr = 7$) is stronger than the flow field for air ($Pr = 0.71$). This Prandtl number influence on the flow field is contributed by the fact that the buoyancy

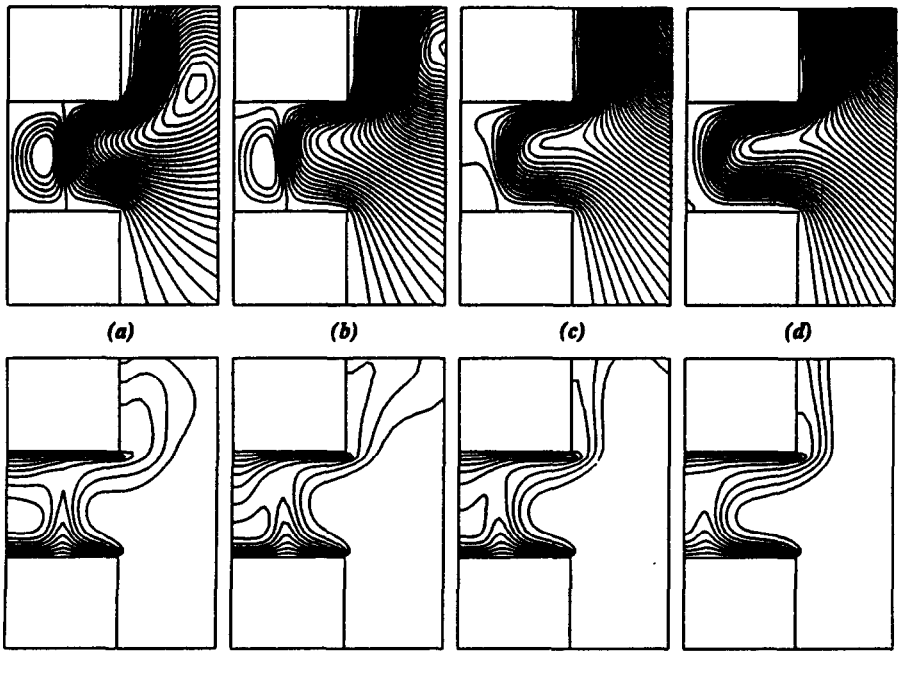


FIG. 8. Streamlines and isotherms for $\theta_2 = 1$, $A = 0.5$, $Pr = 0.71$, $Ra = 10^5$ at: (a) $\tau = 21\Delta\tau$, (b) $\tau = 26\Delta\tau$, (c) $\tau = 31\Delta\tau$, (d) $\tau = 36\Delta\tau$.

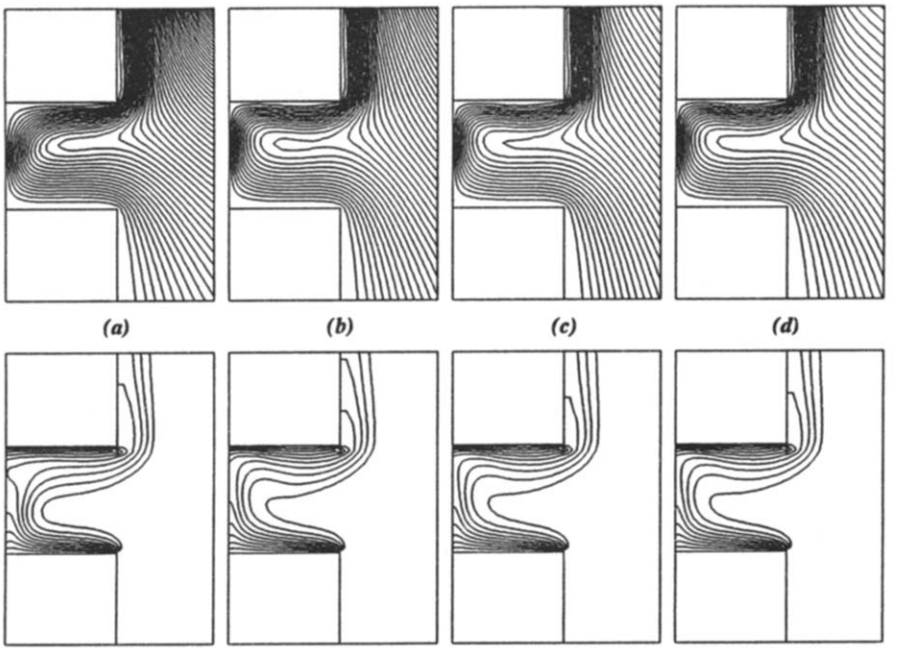


FIG. 9. Streamlines and isotherms for $\theta_2 = 1$, $A = 0.5$, $Pr = 0.71$, $Ra = 10^5$ at: (a) $\tau = 40\Delta\tau$, (b) $\tau = 60\Delta\tau$, (c) $\tau = 120\Delta\tau$, (d) $\tau = 260\Delta\tau$.

parameter ($g\beta/\alpha\nu$) of the water is almost one order of magnitude higher than that of the air.

As $Pr$ increases (0.71–7), the cold fluid enters the open cavity at higher speeds and penetrates further inside as shown in Fig. 10(b). Comparison of the isotherms in Figs. 10(a) and (b) indicates that the thermal boundary layer along the lower block becomes thinner yielding higher heat transfer rates for higher Prandtl numbers. The above-mentioned comparison also indicates that the thermally stratified region along the upper block becomes more apparent with an increase in $Pr$. As illustrated in Fig. 10(b), an

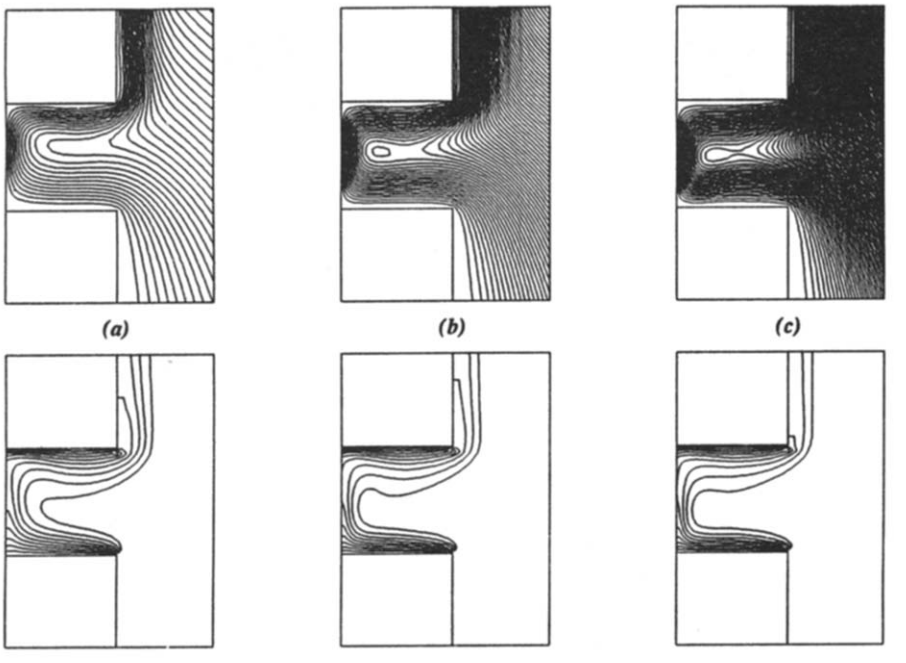


FIG. 10. Streamlines and isotherms for $\theta_2 = 1$, $A = 0.5$, $Ra = 10^5$: (a) $Pr = 0.71$, (b) $Pr = 7$, (c) $Pr = 100$ at steady state.

increase in the Prandtl number significantly increases the wall plume thickness while decreasing its average temperature. Figure 10(b) also illustrates the formation of a vortex which is caused by stronger viscous interactions between the incoming and outgoing flows. The above-mentioned characteristics are further pronounced as the Prandtl number is increased from 7 to 100 as can be seen in Fig. 10(c). In the case of $Pr = 100$, the additional, viscous damping caused by an increase in Prandtl number has an amplifying effect on the stratification. This phenomenon can be clearly seen by the depicted flow field in Fig. 10(c) and is expected to cause an earlier incidence of instabilities for higher Prandtl number fluids.

### 3.4. *The effects of temperature ratio*

The effects of different temperature ratios between the two blocks on the flow field and the temperature distribution inside the open cavity were studied for the general case of the lower block temperature of $\theta_1 = 1$, an aspect ratio of $A = 0.5$, $Pr = 0.71$, and $Ra = 10^5$. The streamlines and isotherms for the cases of the upper block temperatures of $\theta_2 = 0.5$, 1, and 2 are presented in Figs. 11(a)–(c). The results for different upper block temperatures illustrate essentially the same characteristics as were observed earlier for the case of $\theta_2 = 1$. As seen from Fig. 11, there is no appreciable change in the entire flow field except for the presence of higher buoyancy forces for higher values of $\theta_2$. This in turn causes the outgoing flow to rise up at greater speeds, thus resulting in a thinner wall plume. Because of higher temperatures associated with the outgoing flow, the average plume temperature also increases as $\theta_2$ increases. Comparison of the results in Fig. 11 shows that the thermally stratified region along the upper block becomes more established as the upper block temperature is increased. As presented by the isotherms in Fig. 11, there is hardly any significant change in heat transfer from the lower block while the heat transfer from the upper block is greatly enhanced due to an increase in the upper block temperature.

Due to a large temperature drop across the thermal boundary layer for $Ra = 10^5$, the fluid with dimensionless temperature range of $\theta \geqslant 0.5$ is confined within the thermal boundary layer along the lower block for all the cases considered in Fig. 11. Therefore, the heat transfer continues to occur from the upper block to the fluid inside the open cavity even when the upper block temperature is $\theta_2 = 0.5$. This is because the rest of the fluid within the open cavity has a temperature range of $\theta < 0.5$ as shown by the isotherms in Fig. 11(a). However, this situation changes drastically for lower Rayleigh numbers such as $Ra = 10^4$. For this Rayleigh number and the upper block temperature of $\theta_2 = 0.5$, first the heat transfer occurs from the upper block to the fluid inside the open cavity since the average temperature of the fluid within the cavity is lower than that of the upper block. But, for larger times, the fluid inside the open cavity warms up and since the thermal boundary layer formation does not happen (for $Ra = 10^4$), the temperature of the fluid in the upper part of the open cavity continues to increase in time until it becomes higher than the upper block temperature. As a result, the direction of the heat transfer is reversed and heat is transferred from

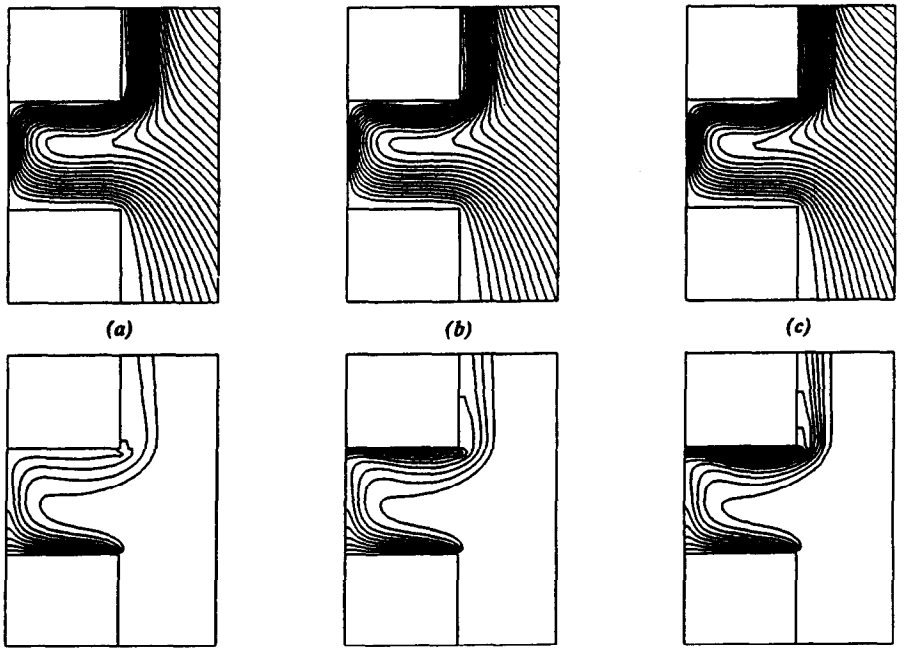


FIG. 11. Streamlines and isotherms for $A = 0.5$, $Pr = 0.71$, $Ra = 10^5$: (a) $\theta_2 = 0.5$, (b) $\theta_2 = 1$, (c) $\theta_2 = 2$ at steady state.

the fluid to the upper block from that time up to and including the steady state. This phenomenon has been confirmed by our numerical experiments.

### 3.5. *The effects of aspect ratio*

Four different aspect ratios were considered to study their influence on the heat transfer characteristics and the flow field in an open-ended cavity. The numerical runs were carried out for the general case of the lower and upper block non-dimensional temperatures of 1, Rayleigh number of $Ra = 10^5$, and using air as the working fluid. The streamlines and isotherms for aspect ratios of $A = 0.25$, 0.5, 1, and 2 are presented in Figs. 12(a)–(d), respectively. As the aspect ratio decreases, the speed of the incoming fluid increases and the thickness of the thermal boundary layer keeps on increasing until it can no longer be considered as a thermal boundary layer. This increase in the thermal boundary layer can be seen in Fig. 12 for both the upper and lower blocks, though the increase in the thermal boundary layer for the lower block seems to be more pronounced. It also shows that, for higher aspect ratios, the bulk of heat transfer is more confined within the vicinity of the blocks leaving much of the open cavity filled with the lower temperature fluids. Furthermore, the formation of the thermally stratified region along the upper block becomes more established for cases with higher aspect ratios as illustrated by the isotherms in Fig. 12(d).

### 3.6. *Heat transfer results*

The cavity Nusselt number defined as the sum of the lower block and the upper block Nusselt numbers was determined by numerical integration of the given expression. Figures 13(a) and (b) provide the time history of the lower block, upper block, and the cavity Nusselt number for Rayleigh numbers of $10^4$ and $10^5$, respectively. The numerical results were obtained for the cases with the lower and upper block temperatures of 1, aspect ratio of 0.5, and air as the working fluid. As indicated by the above figures, an overshooting of the maximum Nusselt number for both blocks above their corresponding steady state values is observed. These overshootings are followed by damped oscillations (these oscillations are more pronounced for $Ra = 10^5$) around their steady state values. The nature of these type of oscillations and their relation with a central vortex oscillation inside the cavity are thoroughly analyzed in ref. [9].

The lower block Nusselt number is greater than the upper Nusselt number for the case of $Ra = 10^4$ while for $Ra = 10^5$, the upper block $Nu$ has the higher value as seen in Fig. 13(b). This very interesting phenomenon can be explained through a chain of physical events based on Figs. 4(b) and 5(a). First, because of the relatively small driving forces associated with the case of $Ra = 10^4$, the thermal boundary layer along the lower block is not fully established. This causes a rise in temperature of the fluid everywhere in the lower half of the open cavity. It should be noted that, the heat transfer from the upper block is mainly by conduction in the thermally stratified region. Therefore, for the case of $Ra = 10^4$, when an already preheated flow from the lower block which is established as a result of this overall temperature rise, passes over the upper block, its heat removal potential is decreased. Consequently, because of smaller vertical temperature

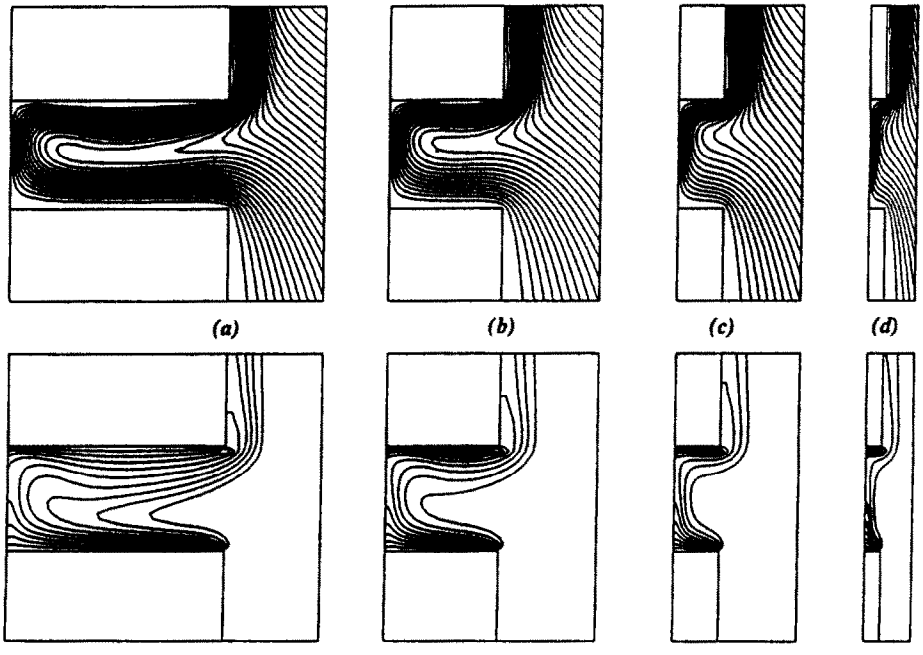


FIG. 12. Streamlines and isotherms for $\theta_2 = 1$, $Pr = 0.71$, $Ra = 10^5$: (a) $A = 0.25$, (b) $A = 0.5$, (c) $A = 1$, (d) $A = 2$ at steady state.

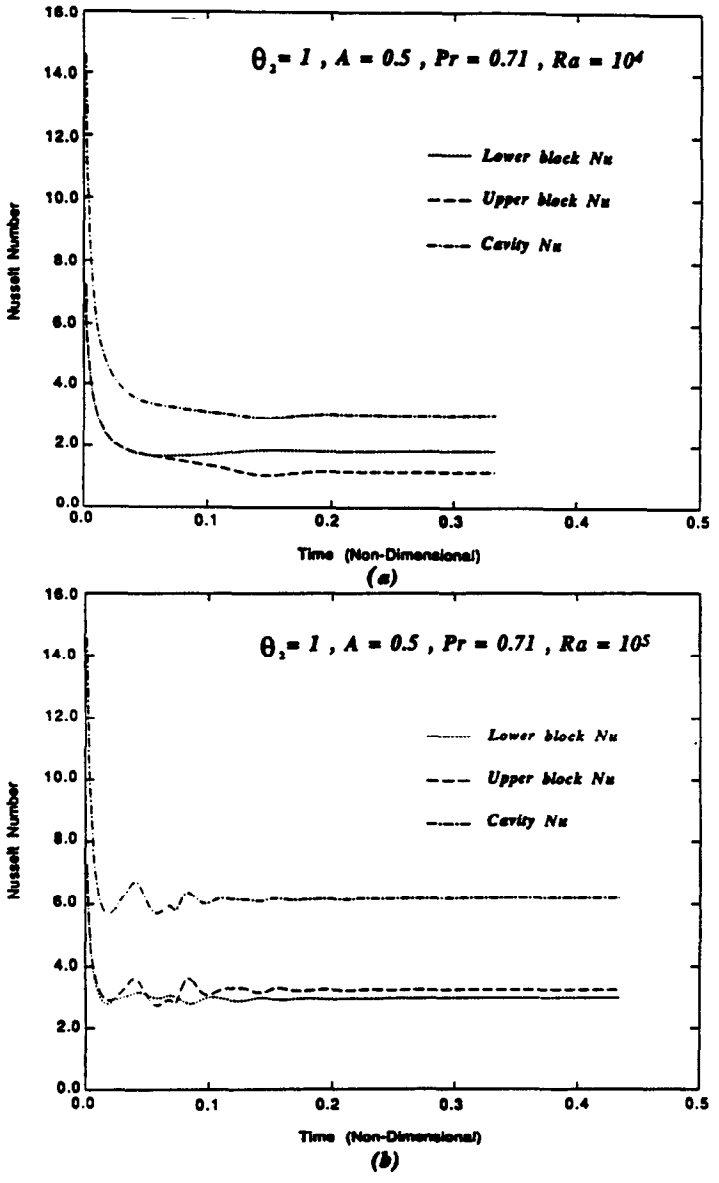


FIG. 13. Time history of the lower block, upper block, and the cavity Nusselt numbers for $\theta_2 = 1$, $A = 0.5$, $Pr = 0.71$: (a) $Ra = 10^4$, (b) $Ra = 10^5$.

gradients along the upper block than the corresponding ones along the lower block, the upper block Nusselt number becomes less than the lower block Nusselt number. However, as the Rayleigh number increases ($Ra = 10^5$), the thermal boundary layer along the lower block becomes more pronounced. It is within this layer that most of the heat transfer takes place leaving part of the open cavity filled with the colder incoming fluid. Therefore, the temperature drop in the thermally stratified region along the upper block becomes more pronounced as it can be seen by the presence of almost four isotherms in the stratified region for the case of $Ra = 10^5$ as compared to the two isotherms present in the case of $Ra = 10^4$. This effect in turn causes the vertical temperature gradient along the upper block to be greater than that of the lower block. Hence, the upper block Nusselt number becomes higher than the lower block Nusselt number for $Ra \geqslant 10^5$. Also as expected, the initial overshoot in the cavity Nusselt number starts earlier in time and is steeper for higher Rayleigh numbers. This is because the time that it takes to heat up the fluid particles along the lower block is decreased, due to steeper temperature gradients, as the Rayleigh number is increased.

Figure 13(b) also depicts the oscillations that occur in the Nusselt number variations as a function of time. As discussed earlier, these oscillations in the time history of Nusselt numbers are due to the existence of thermal instabilities caused by the two driving mech-

anisms acting on the incoming flow in the early stages of the flow development. As it can be seen, the amplitude of oscillations is higher for the upper block Nusselt number compared to the corresponding values for the lower block. The increase in amplitude is because the flow along the upper block starts after the flow has passed over the lower block. Therefore, the instabilities which had been introduced after the flow had passed over the lower block are further increased when the flow passes over the upper block.

Figure 14 presents the Prandtl number effects on heat transfer characteristics of the natural convection in an open-ended cavity. The time history of the cavity Nusselt number is obtained for the cases with the lower and upper block temperatures of 1, aspect ratio of 0.5, Rayleigh number of $10^5$, and three different Prandtl numbers. The same phenomenon of an overshooting of the cavity Nusselt number followed by damped oscillations around a steady state value is also observed for cases with higher Prandtl numbers. As it can be seen from Fig. 14, the initial overshoot of the cavity Nusselt number becomes steeper and starts earlier in time for higher Prandtl number cases. This is expected since as a result of higher velocities associated with the incoming flow for higher Prandtl numbers, the heating period of the fluid particles traveling along the lower block decreases. An interesting phenomenon which is clearly depicted in Fig. 14, is that while the Nusselt number becomes steeper and starts its overshoot earlier in time, the damping of the oscillations, due to the stronger viscous forces becomes more effective for higher Prandtl numbers.

Figure 15(a) presents the time history of the cavity Nusselt number for different temperature ratios. As can be seen from Fig. 15(a), the cavity Nusselt number increases as the upper block temperature increases. However, interestingly enough, the frequency and the amplitude of oscillations in the cavity Nusselt number decreases resulting in an earlier approach to steady state for higher values of $\theta_2$. The reason for the aforementioned behavior can be traced back to the presence of a more pronounced thermally stratified region along the upper block for the higher values of $\theta_2$. Therefore, in essence, for the higher values of $\theta_2$, the more established stratified region has a more stabilizing effect on the flow which is passing through the cavity. The influence of aspect ratio on the heat transfer characteristics within the cavity is shown in Fig. 15(b). The results show that, as the aspect ratio increases the cavity Nusselt number increases. As seen from Fig. 15(b), the period of time for the oscillations decreases while the amplitude of the oscillations increases with an increase in aspect ratio.

Table 1 presents a summary of the lower block, upper block, and the cavity Nusselt numbers at steady state and pseudo steady state cases. As clearly shown by the tabulated results, the cavity Nusselt number increases with an increase in Rayleigh number, an increase in Prandtl number, an increase in temperature ratio, and an increase in aspect ratio. This trend is followed by both the upper block and the lower block Nusselt numbers. It should be mentioned that as the temperature ratio increases, the heat transfer from the upper block increases significantly because of the larger vertical temperature gradients along the upper block while the heat transfer from the lower block remains almost unchanged. This can be traced back to the flow over the lower block which does not experience any noticeable changes as the upper block temperature increases. Hence, the vertical temperature gradients along the lower block do not change significantly as seen in Figs. 11(a)–(c).

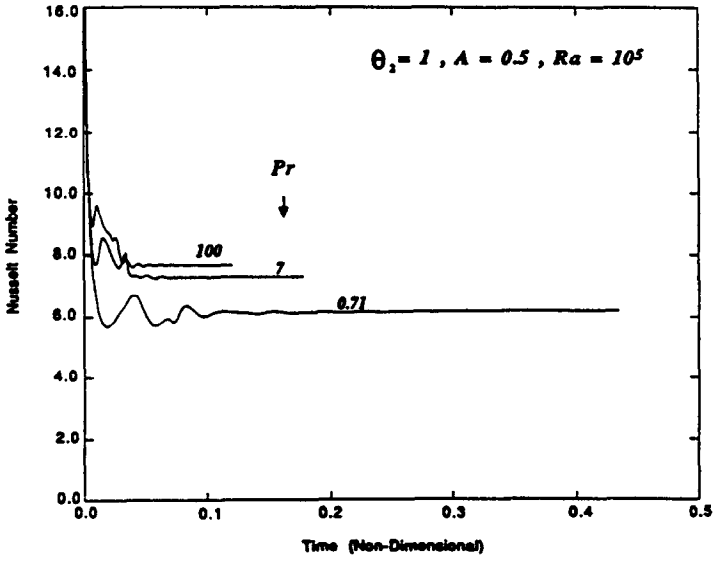


FIG. 14. Time history of the cavity Nusselt number for $\theta_2 = 1$, $A = 0.5$, $Ra = 10^5$ and $0.71 \leqslant Pr \leqslant 100$.

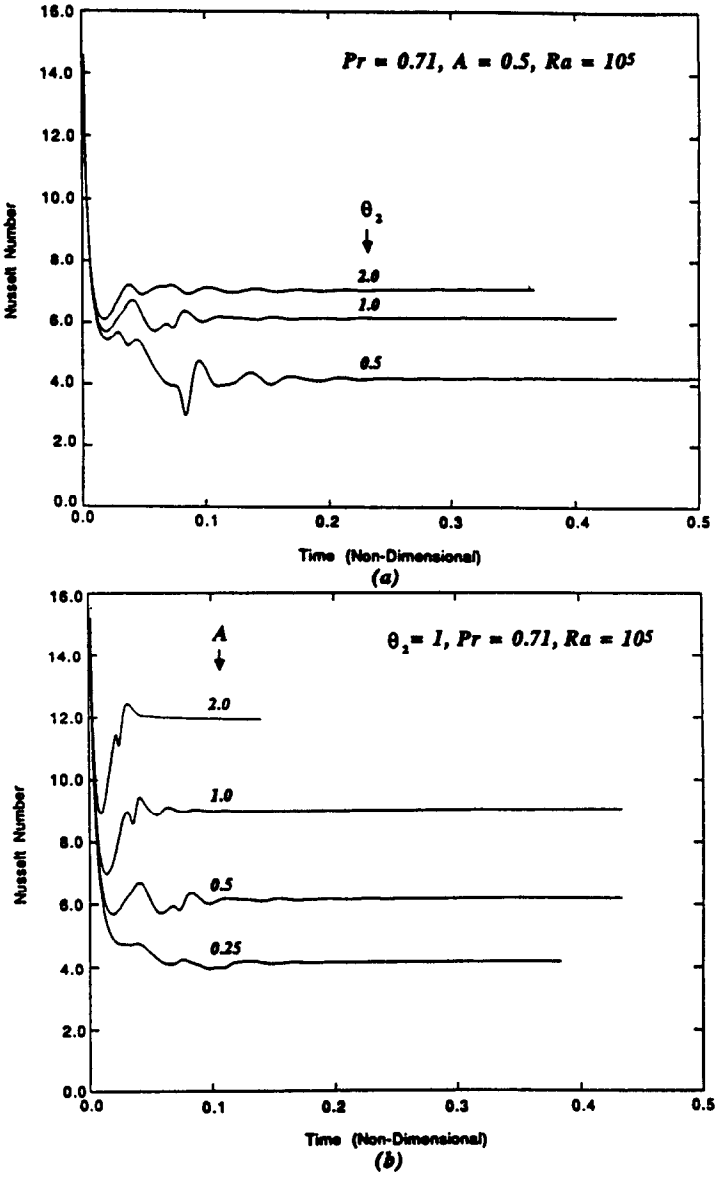


FIG. 15. Time history of the cavity Nusselt number for $Pr = 0.71$, $Ra = 10^5$: (a) $A = 0.5$ and $0.5 \leqslant \theta_2 \leqslant 2$; (b) $\theta_2 = 1$ and $0.25 \leqslant A \leqslant 2$.

## 4. COMPARISONS

The validity and the accuracy of the numerical scheme were checked against two different sets of problems. These were the buoyancy-driven flow in enclosures with differentially heated walls and the natural convection in square open cavities with insulated top and bottom walls. In the first case, the results for Rayleigh numbers of up to $10^6$ are compared with the benchmark solution prepared by De Vahl Davis [10]. The qualitative agreement of the calculated maximum stream function and the Nusselt number with those of the benchmark solution was very good. Comparisons were also done for a range of different Prandtl numbers and aspect ratios. This was done by using the heat transfer relationship reported by Catton [11]. This relationship is one of the few reliable correlations that incorporates Prandtl number effects. Again, our calculated Nusselt numbers compared quite favorably with the above-mentioned correlation. Comparison for the first set of problems were also made for a range of Rayleigh numbers that were higher than those commonly reported in the literature. The streamline contours and isotherms for $Ra = 4 \times 10^8$ showed a very good qualitative agreement with the corresponding contours reported in Paolucci and Chenoweth [12].

In the second set of problems, comparisons were first made with the work of Chan and Tien [3] for a

Table 1. Cavity Nusselt number as a function of relevant parameters

| | | $A = 0.25$ | $A = 0.5$ | | | $A = 1$ | $A = 2$ |
|---|---|---|---|---|---|---|---|
| $Ra$ | $Pr$ | $\theta_2 = 1$ | $\theta_2 = 0.5$ | $\theta_2 = 1$ | $\theta_2 = 2$ | $\theta_2 = 1$ | $\theta_2 = 1$ |
| $10^3$ | 0.71 | | | 1.263[a] | | | |
| | | | | 0.826[b] | | | |
| | | | | 0.437[c] | | | |
| $10^4$ | | | 1.616 | 3.011 | 3.737 | | |
| | | | 1.857 | 1.842 | 1.822 | | |
| | | | −0.241 | 1.169 | 1.915 | | |
| $10^5$ | | 4.176 | 4.232 | 6.197 | 7.116 | 9.088 | 11.952 |
| | | 2.435 | 2.990 | 2.976 | 2.953 | 3.823 | 4.920 |
| | | 1.741 | 1.242 | 3.221 | 4.163 | 5.265 | 7.032 |
| $2 \times 10^5$ | | | | 7.364 | | | |
| | | | | 3.400 | | | |
| | | | | 3.964 | | | |
| $3 \times 10^5$ | | | | 8.042–8.060 | | | |
| | | | | 3.669–3.674 | | | |
| | | | | 4.368–4.389 | | | |
| $5 \times 10^5$ | | | | 8.656–9.812 | | | |
| | | | | 3.990–4.350 | | | |
| | | | | 4.410–5.656 | | | |
| $10^3$ | 7.0 | | | 1.532 | | | |
| | | | | 0.973 | | | |
| | | | | 0.561 | | | |
| $10^4$ | | | | 3.627 | | | |
| | | | | 2.274 | | | |
| | | | | 1.169 | | | |
| $10^5$ | | | | 7.312 | | | |
| | | | | | 3.710 | | |
| | | | | 3.602 | | | |
| $10^4$ | 100 | | | 3.730 | | | |
| | | | | 2.374 | | | |
| | | | | 1.3513 | | | |
| $10^5$ | | | | 7.687 | | | |
| | | | | | 4.174 | | |
| | | | | 3.513 | | | |

[a] The cavity Nusselt number.
[b] The lower block Nusselt number.
[c] The upper block Nusselt number.

range of Rayleigh numbers $Ra \leqslant 10^8$. The numerical results were in very good agreement, both qualitatively and quantitatively with their results for the same range of extensions in the far field boundary conditions. For this type of geometry, qualitative comparisons were also made with the work of Penot [1].

Quantitative comparisons with the experimental correlation presented by Catton [11], numerical solutions given by De Vahl Davis [10] and the numerical solutions presented by Chan and Tien [3] are summarized in Table 2. The experimental correlation given in Catton's [11] work by

$$Nu_L = 0.22\left[\frac{Pr\,Ra_L}{0.2+Pr}\right]^{.28}\left[\frac{H}{L}\right]^{-0.25}$$

for

$$2 < H/L < 10, \quad Pr < 10^5, \quad Ra_L < 10^{10}$$

and De Vahl Davis's [10] numerical results were based on a closed cavity while Chan and Tien's [3] results are based on an open cavity. It should be noted that for the open cavity geometry Chan and Tien's [3] work constituted the only set of results that we could make a quantitative comparison with. We could only make qualitative comparisons with the work of Penot [1] due to a lack of specific information needed to make a quantitative comparison. The same problem existed with the results given by LeQuere *et al.* [2]. For example, in Penot's work [1] there is no explicit information about the Nusselt number distribution or the flow field and though this is the only open cavity work that presents any transient results it contains only one figure which pertains to any type of transient results (with no related discussions). The aforementioned figure cannot really be considered as a transient result since it only presents a qualitative description of the Nusselt number up to just a few $\Delta t$'s. An overall accuracy check was also done on the problem by using the global energy balance. Assuming the temperature gradients and the excess temperatures (above the ambient temperature) around the periphery of the computational domain are negligible and integrating the energy equation from $t = 0$ to $t_{\text{steady state}}$ we were able to show that the overall energy balance is indeed satisfied.

Table 2. Comparisons between related previous experimental and numerical results and the present work

| *Ra* | *Pr* | *H/L* | Source | *Nu* (source) | *Nu* (our results) | Geometry | Percentage difference (%) |
|---|---|---|---|---|---|---|---|
| 489.744 | 0.71 | 4 | [a] | 5.68 | 5.62 | Cavity | 1.06 |
| 785.904 | 0.71 | 4 | [a] | 6.49 | 6.48 | Cavity | 0.15 |
| 1 056 267 | 0.71 | 4 | [a] | 7.05 | 7.09 | Cavity | 0.56 |
| 1 000 | 1 | 1 | [b] | 1.117 | 1.116 | Cavity | 0.09 |
| 10 000 | 1 | 1 | [b] | 2.238 | 2.242 | Cavity | 0.18 |
| 100 000 | 1 | 1 | [b] | 4.509 | 4.522 | Cavity | 0.29 |
| 1 000 000 | 1 | 1 | [b] | 8.817 | 8.85 | Cavity | 0.39 |
| 1 000 | 1 | 1 | [c] | 1.07 | 1.07 | Open cavity | 0 |
| 10 000 | 1 | 1 | [c] | 3.41 | 3.44 | Open cavity | 0.88 |
| 100 000 | 1 | 1 | [c] | 7.69 | 7.78 | Open cavity | 1.15 |
| 1 000 000 | 1 | 1 | [c] | 15 | 15.5 | Open cavity | 3.3 |
| 10 000 000 | 1 | 1 | [c] | 28.6 | 29.6 | Open cavity | 3.5 |
| 100 000 000 | 1 | 1 | [c] | 56.8 | 57.6 | Open cavity | 1.4 |

[a] Experimental correlations (Catton [11]).
[b] Numerical solutions from DeVahl Davis [10].
[c] Numerical solutions from Chan and Tien [3].

## 5. CONCLUSIONS

The transient behavior of the flow field and the heat transfer characteristics inside the open-ended cavity and its surroundings are thoroughly investigated in this work. The influences of the external corners on the flow pattern and the heat transfer process and the importance of the far field boundary conditions, their extensions, and the interaction between the controlling parameters are explored.

The numerical results show that the flow characteristics are quite sensitive to the location where the boundary conditions are applied. It was found that the extent of the enlarged computational domain has a more pronounced effect on the results than earlier anticipated by other investigators. The results show that the flow and heat transfer characteristics inside the open-ended cavity and in its immediate surroundings do not change significantly provided that the computational domain is extended at least 60 times the cavity height for cases with high Rayleigh numbers. The significant effect of the sharp corners on the flow field and heat transfer process in the open-ended cavity is shown via the vorticity generation and the introduction of the flow instabilities.

The transient behavior of the flow field is characterized by the secondary recirculating flow formation along the lower block in addition to the primary flow inside the open-ended cavity. The creation of the secondary recirculating flow and the primary flow, their interactions, fluctuations in their strengths, and their approach towards the steady state are discussed at length. The opposing interactions between the 'suction mechanism' and the 'buoyant mechanism' leading to the introduction of oscillation in the heat transfer process are analyzed. The transient results show that the damping of the oscillations decreases with an increase in Rayleigh number while it increases for larger Prandtl numbers. The transient results also show that the frequency and amplitude of the oscillations in the heat transfer process decrease with an increase in the upper block temperature. Furthermore, it is also found that the amplitude of oscillations increase with an increase in the aspect ratio.

## REFERENCES

1. F. Penot, Numerical calculation of two-dimensional natural convection in isothermal open cavities, *Numer. Heat Transfer* **5**, 421–437 (1982).
2. O. LeQuere, J. A. C. Humphrey and F. S. Sherman, Numerical calculation of thermally driven two-dimensional unsteady laminar flow in cavities of rectangular cross section, *Numer. Heat Transfer* **4**, 249–283 (1981).
3. Y. L. Chan and C. L. Tien, A numerical study of two-dimensional natural convection in square open cavities, *Numer. Heat Transfer* **8**, 65–80 (1985).
4. J. Ettefagh and K. Vafai, Natural convection in open-ended cavities with a porous obstructing medium, *Int. J. Heat Mass Transfer* **31**, 673–693 (1988).
5. P. J. Roache, *Computational Fluid Dynamics*. Hermosa, Albuquerque (1976).
6. A. Thom and C. J. Apelt, *Field Computations in Engineering and Physics*. Van Nostrand (1961).
7. P. J. Roache and T. J. Mueller, Numerical solutions of laminar separated flows, *AIAA J.* **8**, 530–538 (1970).
8 S. C. Kacker and J. H. Whitelaw, Prediction of wall-jet and wall-wake flows, *J. Mech. Sci.* **12**, 404–420 (1970).
9. K. Vafai and J. Ettefagh, Thermal and fluid flow instabilities in buoyancy-driven flows in open-ended cavities, *Int. J. Heat Mass Transfer* **33**, 2329–2344 (1990).
10. G. De Vahl Davis, Natural convection of air in a square cavity: a bench mark numerical solution, *Int. J. Numer. Meth. Fluids* **3**, 249–264 (1983).
11. I. Catton, Natural convection in enclosures, *Proc. Sixth Int. Heat Transfer Conf.*, Toronto, 1978, Vol. 6, pp. 12–35. National Research Council of Canada (1978).
12. S. Paolucci and D. R. Chenoweth, Transition to chaos in a differentially heated vertical cavity, *J. Fluid Mech.* **201**, 379–410 (1989).

## EFFET DES BORDS EFFILES ET DES CONDITIONS AUX LIMITES SUR LES ECOULEMENTS FLOTTANTS

**Résumé**—On discute des effets des bords effilés et des conditions aux limites éloignées sur la génération des tourbillons et des instabilités. L'importance des conditions aux limites et l'interaction entre les variables opératoires sont discutées et une analyse en profondeur est présentée pour l'écoulement du fluide et l'interaction des tourbillons dans une cavité ouverte. La formation d'une région stratifiée thermiquement et son rôle dans les instabilités thermiques sont discutés. Le comportement variable du champ d'écoulement, à travers la formation des tourbillons et les interactions en opposition, est étudié à travers les mécanismes de flottement et de succion qui conduisent à un vortex central oscillant, à une survitesse et à des oscillations dans les mécanismes thermiques. Enfin, les effets des paramètres géométriques et thermophysiques ainsi que l'influence du nombre de Rayleigh et de niveaux différents de température sont étudiés à fond.

## EINFLUS VON SCHARFEN ECKEN AUF FREIE KONVEKTIONSSTRÖMUNGEN UNTER BESONDERER BERÜCKSICHTIGUNG DER ÄUSSEREN BERANDUNG

**Zusammenfassung**—Der Einfluß von scharfen Ecken und der Randbedingungen auf die Wirbelbildung und Strömungsinstabilitäten wird untersucht. Ausführlich wird auf die Bedeutung der Randbedingungen und die Wechselwirkung zwischen den Kontrollvariablen eingegangen. Eine tiefgreifende Analyse der gegenseitigen Beeinflussung von Strömung und Wirbelbildung in einem offenen Kanal wird präsentiert. Die Ausbildung eines thermisch geschichteten Gebiets und seine Rolle bei der Entstehung von thermischen Instabilitäten wird diskutiert. Das zeitliche Verhalten des Strömungsfeldes bei der Bildung von Wirbeln und den gegensätzlichen Auswirkungen der Auftriebs- und Saugmechanismen, die zu einem oszillierenden Zentralwirbel, einem Überschießen und zu Oszillationen bei der Wärmeübertragung führen, wird analysiert. Abschließend werden sowohl die Einflüsse der geometrischen und thermophysikalischen Parameter als auch der Einfluß der Rayleigh-Zahl und verschiedener Temperaturniveaus umfassend untersucht.

## ИССЛЕДОВАНИЕ ВЛИЯНИЯ ОСТРЫХ УГЛОВ НА СВОБОДНОКОНВЕКТИВНОЕ ТЕЧЕНИЕ С УЧЕТОМ ВНЕШНИХ ГРАНИЦ

**Аннотация**—Исследуется влияние острых углов и граничных условий в приближении дальнего поля на вихреобразование и неустойчивость течения. Обсуждается роль граничных условий в указанном приближении и взаимодействие между контролирующими величинами, и проводится тщательный анализ течения вихрей в незамкнутых полостях. Изучается образование термически стратифицированной области и ее непосредственное влияние на тепловую неустойчивость. Анализируются нестационарность поля течения в процессе вихреобразования и противодействие подъемной силы и отсоса, проводящих к возникновению пульсирующего центрального вихря, а также к варьированию и колебаниям процесса теплопереноса. Подробно исследуются а также числа Рэлея и различных уровней температур.